Model for quantitative analysis of reflection-electron-energy-loss spectra

F. Yubero* and S. Tougaard
Fysisk Institut, Odense Universitet, DK-5230 Odense M, Denmark
(Received 12 November 1991)

Two models to reproduce experimental inelastic-electron-scattering cross sections determined from reflection-electron-energy-loss spectroscopy (REELS) are considered. The models take into account the momentum transfer in the inelastic processes. Inputs for the models are the dielectric function and the inelastic electron mean free path, which are both taken from previous works. It is found that a model that takes into account the k dependence of the dielectric function and the effect of the field set up by the incoming electron on the outgoing electron gives the best description. Without any adjustable parameters, a reasonable quantitative agreement between experimental and theoretical cross sections is found for Al, Ti, Fe, Cu, Pd, Ag, and Au in a wide energy range (175–10 000 eV). For a backscattered electron, the effective inelastic mean free path is found to depend strongly on the path length. A method to determine the dielectric function from REELS spectra is suggested.

I. INTRODUCTION

The aim of this paper is to study the inelastic-scattering properties of low-energy (≤ 10 keV) electrons as they travel in the surface region of solids. This topic is particularly important since the surface electron spectroscopies XPS (x-ray photoelectron spectroscopy), AES (Auger-electron spectroscopy), and REELS (reflection-electron-energy-loss spectroscopy) rely on analysis of energy spectra of electrons in this energy range. For quantitative applications of these spectroscopies, reliable models for the inelastic-scattering cross section are therefore essential.

REELS spectra can easily be measured and the experimental facility is available in most surface-science laboratories.

Information on the inelastic-electron-scattering cross section can be obtained by analysis of REELS spectra.[1,2] Recently, this method was applied[2] to produce experimental cross sections for Cu, Ag, and Au in the energy range 300–2000 eV, and for Si, Ti, Fe, and Pd in the energy range 300–10 000 eV. Considering the importance of quantitative surface analysis by electron spectroscopy, it is essential to look for as simple models as possible to make practical applications feasible. We have therefore considered models of varying degrees of complexity in an attempt to reproduce the effective cross sections determined from the REELS experiments.

For an infinite medium, the cross section $K(E_0, \hbar\omega)$ may be evaluated directly from the complex dielectric function ϵ (Refs. 3–5) by

$$K(E_0, \hbar\omega) = \frac{1}{\pi E_0 a_0} \int \frac{dk}{k} \operatorname{Im}\left\{\frac{1}{\epsilon(k,\omega)}\right\},$$

where E_0 is the primary electron energy and a_0 the Bohr radius. However, this model was found[2] to be insufficient to describe cross sections determined from REELS. The reason is that in REELS, as well as in XPS and AES, the effect of the surface must be included. Models to deter-

mine ϵ from REELS have previously been considered,[6–9] some of which also include the k dispersion in ϵ. The basic assumption in these works is that the combined effect of the surface and the bulk excitations can be modeled by a linear combination of the surface electron-loss function $\operatorname{Im}\{1/(\epsilon+1)\}$ and the bulk electron-loss function $\operatorname{Im}\{1/\epsilon\}$. It has further been suggested[8,10] to determine the surface loss function from an experimental REELS spectrum taken at grazing angle at a low energy, since this will effectively increase the importance of surface excitations.

We have recently attempted to single out the surface and bulk components from sets of spectra taken at widely different energies.[11] It was shown that the shape of the cross sections can be reasonably well described by a linear combination of a pure bulk and a pure surface component. However, it was also shown[11] that the fitting parameters only carry limited quantitative information. Therefore, a simple separation in surface and bulk components is not possible for a quantitative description of the energy-loss processes in REELS.

In the present work, we have developed more realistic models to reproduce quantitatively cross sections determined from REELS experiments.

II. THEORY

We study the problem of an electron traveling in a REELS geometry. We assume a fast electron with velocity $\mathbf{v} = v\hat{\mathbf{x}}$ and energy E_0 coming from the vacuum ($x = -\infty$) to a semi-infinite medium with the surface at $x = 0$. The electron is elastically backscattered at the depth $x = a$ inside the medium, and then leaves the solid along the same path (see Fig. 1).

We want to calculate the effective cross section $K_{\text{eff}}(E_0, \hbar\omega, x_0)$, which we define as the average probability that this electron shall lose energy $\hbar\omega$ ($E_0 \gg \hbar\omega$) per unit energy loss and per unit path length. The average is over the total path length $x_0 = 2a$ traveled by the electron in the solid. In order to simplify the problem, we assume
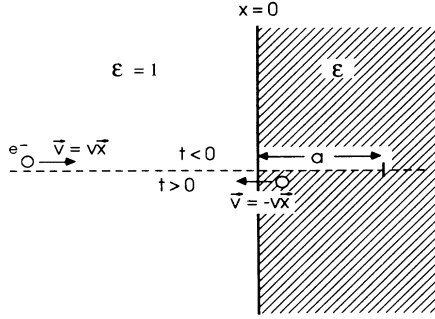
FIG. 1. Geometry considered in the theoretical models. An electron starting at $x = -\infty$ with velocity $\mathbf{v}$ penetrates the surface of the solid (at $x = 0$) and is specularly backscattered at depth $x = a$ and time $t = 0$.

normal incidence and specular reflection in the back-scattering event.

The effective stopping power $S(E_0, x_0)$ for the path x_0 is related to $K_{eff}(E_0, \hbar\omega, x_0)$ as follows:

$$S(E_0, x_0) = \int_0^\infty \hbar\omega K_{eff}(E_0, \hbar\omega, x_0)\, d(\hbar\omega) . \tag{1}$$

On the other hand, we can calculate this stopping power from the relation

$$S(E_0, x_0) = \frac{1}{x_0} \int_{-\infty}^\infty \mathbf{v} \cdot \mathbf{F}\, dt , \tag{2}$$

where

$$\mathbf{F} = -\int \rho_{ext}(\mathbf{r}, t) \nabla \Phi_{ind}(\mathbf{r}, t) \cdot d\mathbf{r} \tag{3}$$

is the force acting on the electron,

$$\Phi_{ind}(\mathbf{r}, t) = \frac{1}{(2\pi)^4} \int_{-\infty}^\infty d\omega \int d\mathbf{k}\, \Phi_{ind}(\mathbf{k}, \omega) e^{i(\mathbf{k}\cdot\mathbf{r} + \omega t)} \tag{4}$$

is the induced potential by the fast electron, and $\rho_{ext}(\mathbf{r}, t)$ is the charge distribution of the electron. Then, from Eqs. (1)–(4), we get, after application of the property $\Phi_{ind}(\mathbf{k}, \omega) = \Phi_{ind}^*(-\mathbf{k}, -\omega)$,

$$K_{eff}(E_0, \hbar\omega, x_0) = \frac{-2\mathbf{v}}{\hbar^2\omega x_0} \frac{1}{(2\pi)^4} \int d\mathbf{k} \int d\mathbf{r} \int dt\, \rho_{ext}(\mathbf{r}, t) \Phi_{ind}(\mathbf{k}, \omega) \nabla e^{i(\mathbf{k}\cdot\mathbf{r} + \omega t)} . \tag{5}$$

So, to solve the problem we have to find Φ_{ind}. This can be done, following the previous work of Ritchie,[4] by solving the Poisson equation

$$\epsilon(\omega) \nabla^2 \Phi_{ind} = -4\pi\rho_{ext} , \tag{6}$$

where

$$\epsilon(\omega) = 1 - \frac{\omega_p^2}{\omega^2 - i\gamma\omega} \tag{7}$$

in the case of a pure free-electron metal (like Al), and more generally[10]

$$\epsilon(\omega) = 1 - \frac{f_0\omega_p^2}{\omega^2 - i\gamma_0\omega} - \sum_{j=1}^n \frac{f_j\omega_p^2}{\omega^2 - \omega_j^2 - i\gamma_j\omega} , \tag{8}$$

where ω_p is the plasmon energy, γ_0 is the reciprocal of the relaxation time of the electrons in the valence band, and f_0 is an oscillator strength that describes the free-electron contribution to $\epsilon(\omega)$. The last term represents the contribution of the interband transitions of energy ω_j, oscillator strength f_j, and lifetime $1/\gamma_j$. To solve Eq. (6), we use the appropriate continuity conditions for the potential and the field at the boundary of the semi-infinite medium.

One might expect some influence from the interference of the field from the incoming electron on the outgoing electron. To be able to study this effect separately, we have therefore considered two models which correspond to two different representations of the primary electrons.

Model A. In this model, we separate the electron tra-jectory into an incoming and an outgoing part. Thus we first find the energy lost by the fast electron according to the charge distribution

$$\rho_{ext\,A-}(\mathbf{r}, t) = \begin{cases} -e\delta(x - a - vt)\delta(y)\delta(z) & \text{if } t < 0 \\ 0 & \text{if } t > 0 \end{cases} \tag{9a}$$

to later do the same for the charge distribution

$$\rho_{ext\,A+}(\mathbf{r}, t) = \begin{cases} 0 & \text{if } t < 0 \\ -e\delta(x - a + vt)\delta(y)\delta(z) & \text{if } t > 0 , \end{cases} \tag{9b}$$

and we average both results to find the total energy lost by the electron.

Model B. In this model, we consider the total electron trajectory

$$\rho_{extB}(\mathbf{r}, t) = \begin{cases} -e\delta(x - a - vt)\delta(y)\delta(z) & \text{if } t < 0 \\ -e\delta(x - a + vt)\delta(y)\delta(z) & \text{if } t > 0 . \end{cases} \tag{10}$$

In model A, the electron on its way out does not experience the influence of the excited electron sea in the solid by the incoming electron, whereas in model B, it will experience the effect of this field.

The solutions for Φ_{ind} and $K_{eff}(E_0, \hbar\omega, x_0)$ are the following

Model A. From Eqs. (6) and (9a), using the continuity conditions for $\Phi_{ind}(x = 0)$ and $\epsilon\nabla\Phi_{ind}(x = 0)$, we find the following. For $t < 0$,

$$\Phi_{\text{ind}A-}(\mathbf{k},\omega,a)=\frac{k_\perp z_{1-}+ik_x z_{2-}}{k_\perp^2+k_x^2}$$

$$+\frac{k_\perp z_{3-}+ik_x z_{4-}}{k_\perp^2+k_x^2}e^{-ik_x a}$$

$$+\frac{\alpha_- i}{k_x+y}\left\{\frac{1}{\epsilon}-1\right\}[e^{-ik_x a}-e^{iya}]\ ,\quad (11a)$$

where a is the depth reached by the electron, and

$$\alpha_-=\frac{-4\pi e}{v}\frac{1}{k_\perp^2+y^2}\ ,$$

$$y=\frac{\omega}{v}\ ,$$

$$z_{1-}=\alpha_-\frac{1-\epsilon}{\epsilon(1+\epsilon)}\frac{k_\perp-iy}{k_\perp}e^{-k_\perp a}-\alpha_-\frac{(1-\epsilon)^2}{\epsilon(1+\epsilon)}e^{iya}\ ,$$

$$z_{2-}=\alpha_-\left\{\frac{1}{\epsilon}-1\right\}e^{iya}\ ,\qquad\qquad (11b)$$

$$z_{3-}=\alpha_- i\frac{y}{k_\perp}\left\{\frac{1}{\epsilon}-1\right\}\ ,$$

$$z_{4-}=-\alpha_-\left\{\frac{1}{\epsilon}-1\right\}\ ,$$

while $k_\perp$ and k_x are the perpendicular and parallel components of the momentum $\mathbf{k}$ of the fast electron.

For $t>0$, we get from Eqs. (6) and (9b),

$$\Phi_{\text{ind}A+}(\mathbf{k},\omega,a)=\frac{k_\perp z_{1+}+ik_x z_{2+}}{k_\perp^2+k_x^2}$$

$$+\frac{k_\perp z_{3+}+ik_x z_{4+}}{k_\perp^2+k_x^2}e^{-ik_x a}$$

$$+\frac{\alpha_+ i}{k_x-y}\left\{\frac{1}{\epsilon}-1\right\}[e^{-ik_x a}-e^{-iya}]\ ,$$

$$(12a)$$

where a is now the path traveled by the electron to reach the surface and

$$\alpha_+=\frac{-4\pi e}{v}\frac{1}{k_\perp^2+y^2}\ ,$$

$$y=\frac{\omega}{v}\ ,$$

$$z_{1+}=\alpha_+\frac{1-\epsilon}{\epsilon(1+\epsilon)}\frac{k_\perp+iy}{k_\perp}e^{-k_\perp a}-\alpha_+\frac{(1-\epsilon)^2}{\epsilon(1+\epsilon)}e^{-iya}\ ,$$

$$(12b)$$

$$z_{2+}=\alpha_+\left\{\frac{1}{\epsilon}-1\right\}e^{-iya}\ ,$$

$$z_{3+}=-\alpha_+ i\frac{y}{k_\perp}\left\{\frac{1}{\epsilon}-1\right\}\ ,$$

$$z_{4+}=-\alpha_+\left\{\frac{1}{\epsilon}-1\right\}\ .$$

Then, from Eq. (5), we find K_{eff} for the incoming and the outgoing electron, and the effective cross section for the total trajectory is the average of these:

$$K_{\text{eff}}(E_0,\hbar\omega,x_0)=\frac{-2e^2}{\hbar^2 v^2\pi}\text{Re}\left\{i\int dk_\perp\left[\frac{1}{\epsilon}-1\right]\frac{k_\perp}{k_\perp^2+y^2}\right\}$$

$$+\frac{8e^2}{\hbar^2\pi}\frac{1}{2a}\text{Re}\left\{i\int dk_\perp\frac{1-\epsilon}{\epsilon(1+\epsilon)}\frac{k_\perp^2}{(k_\perp^2+y^2)^2}\right\}$$

$$+\frac{-e^2}{\hbar^2 v\omega\pi}\frac{1}{2a}\text{Re}\left\{4i\int dk_\perp\frac{1-\epsilon}{\epsilon(1+\epsilon)}\frac{k_\perp}{(k_\perp^2+y^2)^2}e^{-k_\perp a}[(k_\perp^2-y^2)\sin(ya)+2yk_\perp\cos(ya)]\right\}\ ,\qquad (13)$$

where $x_0=2a$.

Model B. From Eqs. (6) and (10), with the same boundary conditions as above, we get

$$\Phi_{\text{ind}}(\mathbf{k},\omega,a)=\frac{k_\perp z_1+ik_x z_2}{k_\perp^2+k_x^2}+\frac{ik_x z_3}{k_\perp^2+k_x^2}e^{-ik_x a}$$

$$+\frac{\alpha i}{k_x^2-y^2}\left\{\frac{1}{\epsilon}-1\right\}$$

$$\times\{k_x[e^{-ik_x a}-\cos(ya)]+iy\sin(ya)\}\ ,$$

$$(14a)$$

where a is the maximum depth reached by the fast electron inside the medium, and

$$\alpha=\frac{-8\pi e}{v}\frac{1}{k_\perp^2+y^2}\ ,$$

$$y=\frac{\omega}{v}\ ,$$

$$z_1=\alpha\frac{1-\epsilon}{\epsilon(1+\epsilon)}e^{-k_\perp a}-\alpha\frac{(1-\epsilon)^2}{\epsilon(1+\epsilon)}\cos(ya)\ ,\qquad (14b)$$

$$z_2=\alpha\left\{\frac{1}{\epsilon}-1\right\}\cos(ya)\ ,$$

$$z_3=-\alpha\left\{\frac{1}{\epsilon}-1\right\}\ .$$

Finally, from Eq. (5), we have

$$K_{\mathrm{eff}}(E_0,\hbar\omega,x_0)=\frac{-2e^2}{\hbar^2v^2\pi}\mathrm{Re}\left\{i\int dk_\perp\left[\frac{1}{\epsilon}-1\right]\frac{k_\perp}{k_\perp^2+y^2}\right\}$$

$$+\frac{-2e^2}{\hbar^2v\omega\pi}\frac{1}{2_a}\mathrm{Re}\left\{i\int dk_\perp\frac{k_\perp}{(k_\perp^2+y^2)^2}\right.$$

$$\times\left[8yk_\perp\cos(ya)e^{-k_\perp a}\frac{1-\epsilon}{\epsilon(1+\epsilon)}+(k_\perp^2-y^2)\sin(2ya)\left[\frac{1}{\epsilon}-1\right]\right.$$

$$\left.\left.-2yk_\perp e^{-2k_\perp a}\frac{1-\epsilon}{\epsilon(1+\epsilon)}-2yk_\perp\left[\frac{1}{\epsilon}-1\right]\left[1+2\cos^2(ya)\frac{1-\epsilon}{1+\epsilon}\right]\right]\right\}\,,\qquad(15)$$

where again $x_0=2a$.

To evaluate numerically the effective cross sections we need to use the relations

$$k^2=k_\perp^2+\frac{\omega^2}{v^2}\quad\text{and}\quad k\,dk=k_\perp dk_\perp\,.\qquad(16)$$

Then we evaluate the integrals over k between the allowed maximum k_+ and minimum k_- momentum transfer

$$k_\pm=\left[\frac{2m}{\hbar^2}\right]^{1/2}[\sqrt{E_0}\pm\sqrt{E_0-\hbar\omega}]\,.\qquad(17)$$

In the limit $x_0\to\infty$, only the first term in Eqs. (13) and (15) remains, and both models give as expected the bulk value[3,4] for $K_{\mathrm{eff}}(E_0,\hbar\omega,x_0)$. For $x_0\to0$ we find

$$(A)\quad \lim_{x_0\to0}\mathbf{K}_{\mathrm{eff}}(E_0,\hbar\omega,x_0)=0\,,\qquad(18a)$$

$$(B)\quad \lim_{x_0\to0}\mathbf{K}_{\mathrm{eff}}(E_0,\hbar\omega,x_0)$$

$$=\frac{-4e^2}{\hbar^2v^2\pi}\frac{1}{2a}\mathrm{Re}\left\{i\int dk_\perp\frac{k_\perp^2}{(k_\perp^2+y^2)}\frac{1-\epsilon}{1+\epsilon}\right\}\,.\qquad(18b)$$

Thus if the electron does not penetrate the medium ($a=0$), it will not lose any energy in model A, while in model B it will, even for $a=0$, transfer energy to the electrons of the medium.

The constant ϵ is given by Eq. (8). This is the Lorentz approximation for the dielectric constant without k dependence. In accordance with previous works,[12,13] we introduce the k dependence in ϵ by the following approximation:

$$\epsilon(\mathbf{k},\omega)=1-\frac{f_0\omega_p^2}{\omega^2-\omega_k^2-i\gamma_0\omega}-\sum_{j=1}^{n}\frac{f_j\omega_p^2}{\omega^2-\omega_k^2-\omega_j^2-i\gamma_j\omega}\,,\qquad(19)$$

where $\hbar\omega_k=\hbar^2k^2/2m$.

From an experimental REELS spectrum, we can evaluate the single-scattering cross section averaged over all possible electron paths (see Sec. III). To compare with experiment, we therefore need to calculate the corresponding theoretical quantity. The transport mean free path for elastic scattering is much larger than the mean free path λ for inelastic scattering.[1] In REELS, we therefore have to a good approximation the same contribution from electrons that have been backscattered at all depths.[1,2]

We assume that the probability for inelastic electron scattering is proportional to $(1-e^{-x/\lambda})$, where x is the path traveled in the medium. Then the probability that the electron has scattered only once is proportional to $xe^{-x/\lambda}$.[14]

Now, from this and from the effective inelastic-scattering cross section for each path, we can evaluate the single-scattering cross section $K_{\mathrm{sc}}(E_0,\hbar\omega)$, averaged over all electrons paths,

$$K_{\mathrm{sc}}(E_0,\hbar\omega)=\frac{1}{\lambda^2}\int_0^\infty xe^{-x/\lambda}K_{\mathrm{eff}}(E_0,\hbar\omega,x)dx\,.\qquad(20)$$

III. CROSS SECTIONS FROM EXPERIMENTAL REELS

An experimental REELS spectrum $j_1(E)$ has contributions from both single and multiple inelastically scattered electrons. We can remove the multiple-scattering contributions and determine $K_{\mathrm{sc}}(E_0,\hbar\omega)$ by the algorithm developed by Tougaard and Chorkendorff,[1,15]

$$\frac{\lambda L}{\lambda+L}K_{\mathrm{sc}}(E_0,E_0-E)=\frac{1}{c}\left[j_1(E)-\int_E^{E_0}\frac{\lambda L}{\lambda+L}K_{\mathrm{sc}}(E_0,E'-E)j_1(E')dE'\right]\,,\qquad(21)$$

F. YUBERO AND S. TOUGAARD

where $L \approx 2\lambda_1$, λ_1 is the transport mean free path for elastic scattering, $c = \int_{E_0-}^{E_0+} j_1(E) dE$ is the elastic peak area, and $E_0 - E = \hbar\omega$.

Finally, taking tabulated values for $\lambda(E_0)$, and using $\int \lambda(E_0) K_{sc}(E_0,\hbar\omega) d(\hbar\omega) = 1$, we can find the experimental cross section $K_{sc}(E_0,\hbar\omega)$ and compare with the theoretical cross section evaluated by Eq. (20).

IV. RESULTS AND DISCUSSION

A. Aluminum

Figure 2 shows $K_{eff}(E_0,\hbar\omega,x_0)$ for different values of the path $x_0 = 2a$, traveled in the interior of the solid. The peak at ~ 10-eV energy loss which corresponds to surface-plasmon excitations dominates for $x_0 < \lambda$. The peak at ~ 15 eV, which corresponds to bulk-plasmon excitation, dominates for larger path lengths. For model A, the relative strength of surface-to-bulk excitations changes gradually with the path length. For model B, the behavior is quite different. For example, for $E_0 = 300$ eV, the strength of the surface plasmon is higher for $x_0 = 4\lambda$ than for $x_0 = 2\lambda$. For $x_0 = 8\lambda$, the surface and bulk peaks have developed into four peaks. In REELS spectra, these will not be seen as separate peaks, since $K_{sc}(E_0,\hbar\omega)$ is an average over all path lengths.

In Fig. 3, we have calculated an effective inelastic mean free path λ_{eff} according to the following expression:[16,17]

$$\frac{1}{\lambda_{eff}(E_0,x_0)} = \frac{1}{\lambda_v(E_0,x_0)} + \frac{1}{\lambda_c(E_0)} , \qquad (22)$$

where $\lambda_v(E_0,x_0) = [\int K_{eff}(E_0,\hbar\omega,x_0) d\hbar\omega]^{-1}$ and $\lambda_c(E_0)$ are the respective valence-band and core-level contributions to the total $\lambda_{eff}(E_0,x_0)$. The values for $\lambda_c(E_0)$ were taken from Penn.[16,17] For large path lengths, λ_{eff} for the two models A and B approach the same value. This value is, for all energies, identical to within a few percent to the values available in the literature.[18,19] For smaller path lengths, the behavior of models A and B is markedly different. Thus, for $x_0 < \lambda$, model A gives a higher λ_{eff} value, while model B gives a lower λ_{eff} value compared with λ_{eff} for large path lengths. The reason is that, in model B, the electron has a nonvanishing probability for inelastic scattering even when it has not penetrated the surface of the solid $(x_0 \to 0)$, while in model A this electron cannot scatter inelastically [see Eq. (18)]. The origin of this is the interference in model B between the field set up by the incoming electron on the outgoing electron. Another effect of this interference can be seen as a damped oscillating dependence of λ_{eff} on the path x_0 for model B.

Experimental cross sections determined by Eq. (21) are shown in Figs. 4 and 5. The slight negative values of the experimental cross sections in the energy range 20–30 eV and the peak at ~ 31 eV are due to the fact that Eq. (21) does not take the inhomogeneity of the surface into ac-
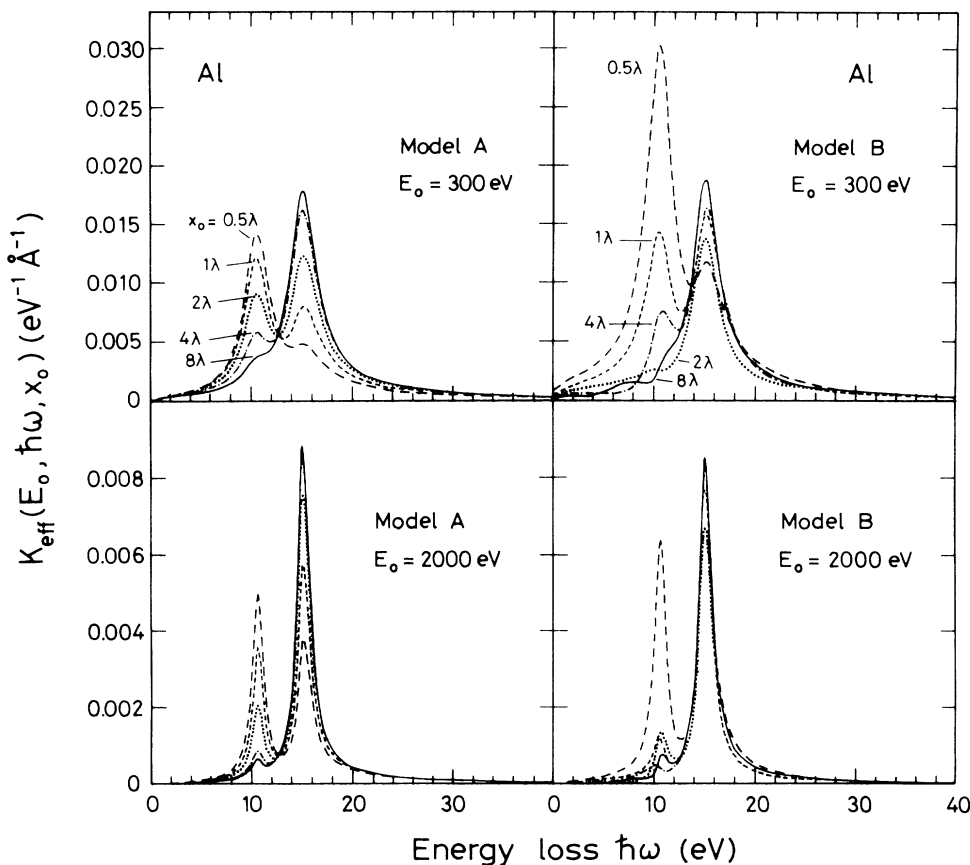

FIG. 2. The effective inelastic-electron-scattering cross section $K_{eff}(E_0,\hbar\omega,x_0)$ for Al at 300 and 2000 eV, calculated by Eq. (13) (model A) and Eq. (15) (model B), respectively. $x_0 = 2a$ is the total path traveled in the solid. Results are shown for different path lengths given in units of λ: 0.5λ (——), 1λ (– – –), 2λ (· · · ·), 4λ (– · — · —), and 8λ (———).
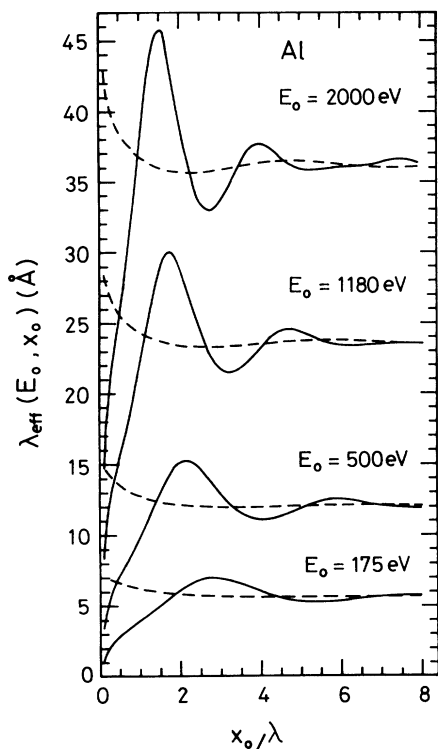
FIG. 3. Effective inelastic mean free paths [Eq. (22)] for electrons backscattered at different depths $a = x_0/2$ in Al. Several primary electron energies E_0 are considered within the two models A (— — —) and B (———).

gave γ_0 values that vary with energy (see Table I). Note that for the theoretical calculations, no further parameters were adjusted, and that the theoretical and experimental cross sections can be compared on an absolute scale. Both the absolute values of $K_{sc}(E_0,\hbar\omega)$ and the relative surface- to bulk-plasmon intensities are much closer to experiment in Fig. 5 than in Fig. 4. It is thus clear that the k dependence of ϵ plays a significant role and must be included.

Comparing now in Fig. 5 the results of models A and B with experiment, we observe that the agreement is clearly better, in particular at low primary energy, for model B. However, model B still does not reproduce all details of the experimental cross sections. For example, the width and intensity of the surface-plasmon peak. The shoulder observed for low primary energies in the experimental cross sections at $\hbar\omega \sim 3$ eV is reproduced by model B, but the intensity is too low. We believe that one of the reasons for these deviations is partly that the actual momentum-transfer dependence of ϵ is more complicated than assumed in Eq. (19). Other sources of error are ap-
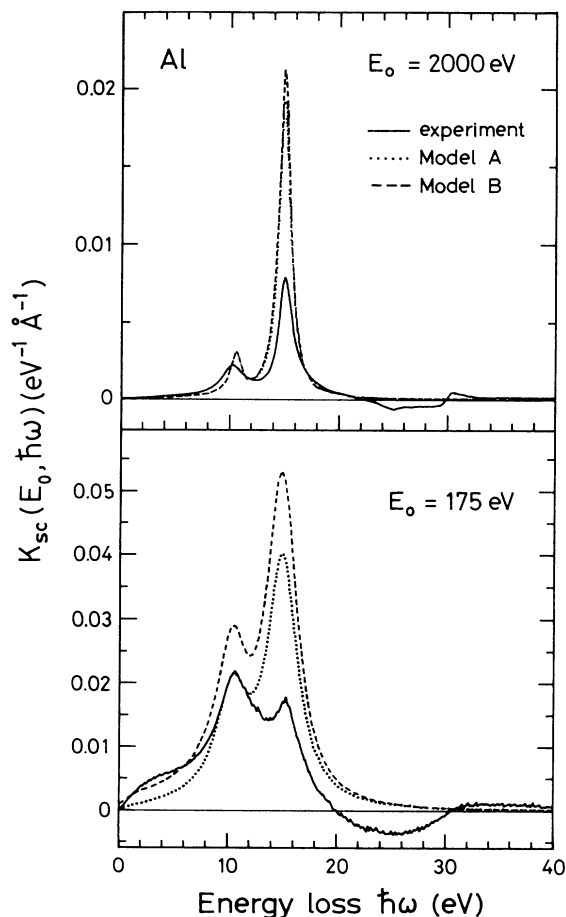
count. This will only affect the values for energies exceeding twice the surface-plasmon energy and the experimentally determined cross sections should therefore only be compared to theory below ~ 18 eV energy loss (see the discussions in Refs. 1 and 15).

For comparison, the effective single-scattering cross section calculated according to Eq. (20), with ϵ given by Eq. (7) (ϵ independent of k), is shown in Fig. 4, and with the k dependence of ϵ given by Eq. (19) (with $f_0 = 1$ and $f_j = 0$ for $j \neq 0$) in Fig. 5. In the theoretical calculations ω_p was adjusted to match the position of the bulk-plasmon peak with experiment. The value was $\omega_p = 15.0$ eV, independent of the primary energy. The parameter γ_0 was adjusted to give a ratio between surface and bulk plasmons as close as possible to the experiment. This

FIG. 4. Theoretical cross sections $K_{sc}(E_0,\hbar\omega)$ neglecting the k dependence of ϵ for the models A and B, compared to experimentally determined cross sections for 175- and 2000-eV energetic electrons in Al.

TABLE I. Values for Al of $\hbar\gamma_0$ used for ϵ in Eq. (19) and inelastic mean free paths λ (Ref. 18), at several primary energies E_0.

E_0 (eV)	$\hbar\gamma_0$ (eV)	λ (Å)
175	3.4	5.6
300	2.8	8.3
500	2.1	12.4
1180	1.5	23.5
2000	1.3	36.0

proximations made in model B, and possible effects of surface roughness on the experimental cross sections.

B. Fe, Ti, Cu, Pd, Ag, and Au

The analysis in Sec. IV A showed that it is essential to include the k dependence of ϵ to quantitatively reproduce
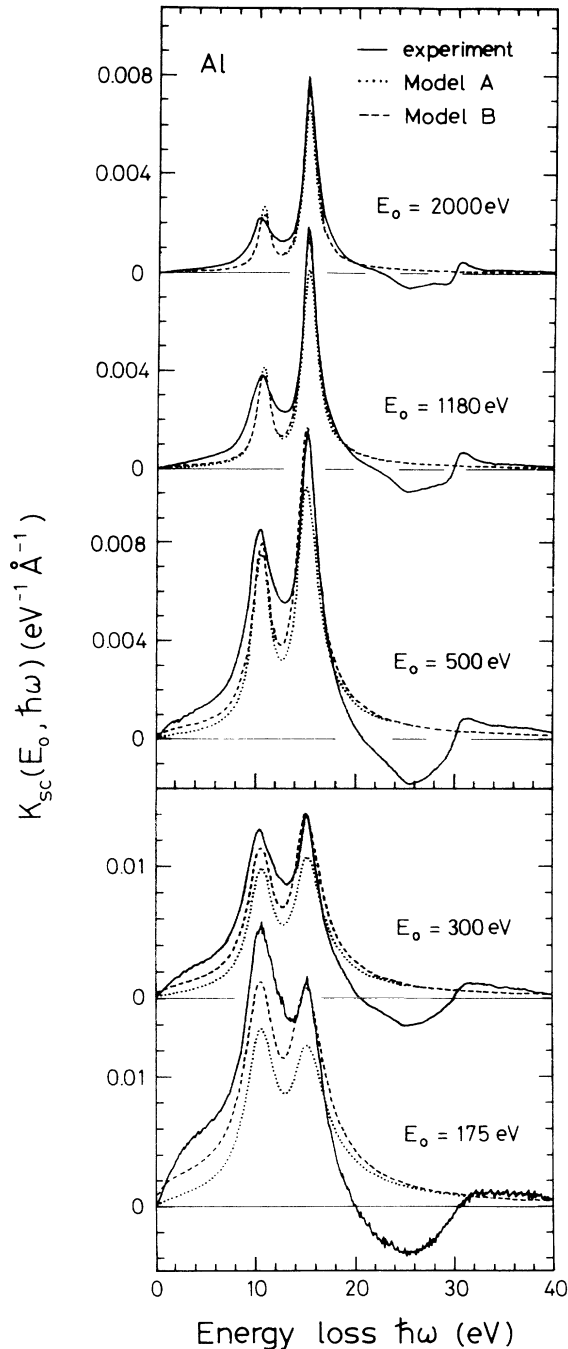

FIG. 5. Theoretical cross sections $K_{sc}(E_0, \hbar\omega)$ for models A and B [Eq. (20)] including k dependence of ϵ according to Eq. (19) compared to experimental cross sections at several energies in Al.

the experimental cross sections. In the following calculations, we have therefore always included the k dependence of ϵ as given by Eq. (19).

The dielectric functions for Fe, Ti, Cu, Pd, Ag, and Au are much more complicated than for Al, because interband transitions play a strong role. For Fe and Pd, ϵ was taken from optical data,[20] while for Ti, Cu, Ag, and Au, it was taken from high-energy thin-film transmission experiments.[21,22] These functions were expanded according to Eq. (19) with $k = 0$. Three to ten terms were used in the expansion to get a satisfactory fit. The expansion coefficients are listed in Table II. The plasmon energy values and the inelastic mean free paths taken from Tanuma, Powell and Penn[19] are listed in Table III.

Figure 6 shows $K_{eff}(E_0, \hbar\omega, x_0)$ for different paths traveled in Fe for both models A and B at $E_0 = 2000$ eV. In model A, K_{eff} changes gradually with the path length. For model B, it is clear that K_{eff} does not consist of just a linear combination of a surface and bulk component, but
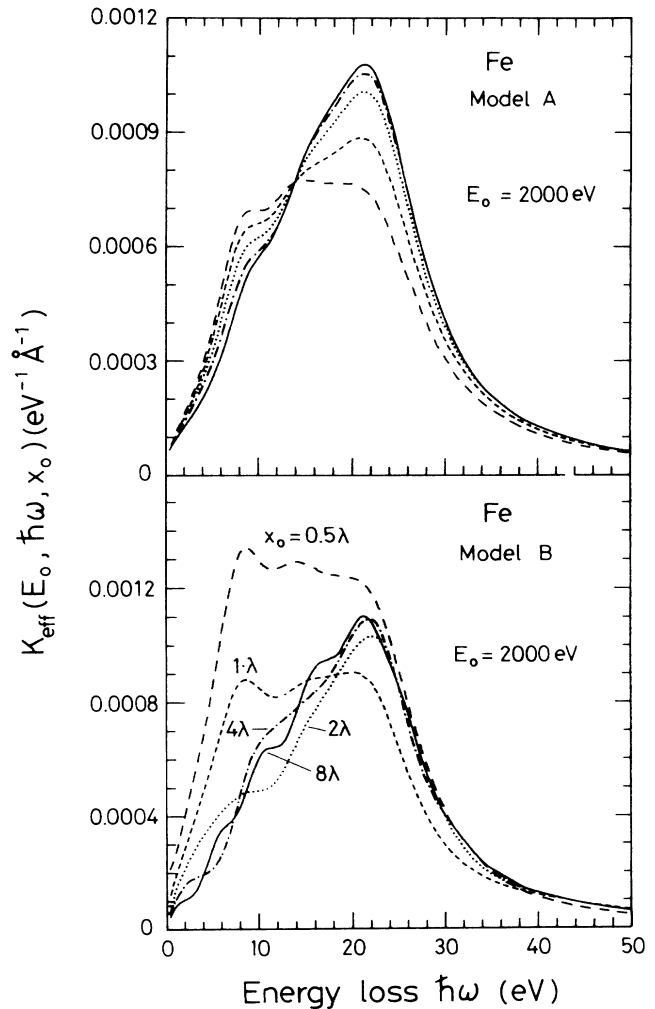

FIG. 6. $K_{eff}(E_0, \hbar\omega, x_0)$ for Fe at 2000 eV, calculated by Eq. (13) (model A) and Eq. (15) (model B), respectively, for several path lengths given in units of λ: 0.5λ (———), 1λ (———), 2λ (· · · ·), 4λ (—·—·—·), and 8λ (———).

of several peaks, the position and width of which varies considerably with the path length. As for Al, the intensity of K_{eff} for short path lengths is higher in model B than in model A. As a result, excitations with energies below 10 eV play a more prominent role in model B than in model A.

In Fig. 7, we show λ_{eff} for Fe [Eq. (22)] for both models at several energies. We have basically the same behavior as for Al, but for Fe the oscillations in λ_{eff} with path length are weaker. The reason is that although the shape of $K_{eff}(E_0, \hbar\omega, x_0)$ for $x_0 > \lambda$ varies considerably with x_0, the area under the curves in Fig. 6 (model B) are almost identical for all $x_0 > \lambda$. Note that the value of λ_{eff} for large x_0 in Fig. 7 (7.9 Å at 300 eV, 34.5 Å at 2000 eV, and 131 Å at 10000 eV) is consistently higher than the values from Tanuma, Powell, and Penn[19] (see Table III).

We believe that the reason is the optical data used here[20] are only available in the energy range 0–30 eV. Thus the contribution to λ_{eff} from the structure around 60-eV energy loss (see Fig. 7 in Ref. 2) has not been included in λ_v. The relative strength of this structure is considerably higher at higher primary energy.[2] This is consistent with the present data, which show the largest deviations in λ_{eff} for the highest primary energies.

Figure 8 shows the theoretical calculations for the cross section $K_{sc}(E_0, \hbar\omega)$ evaluated by Eq. (20) with
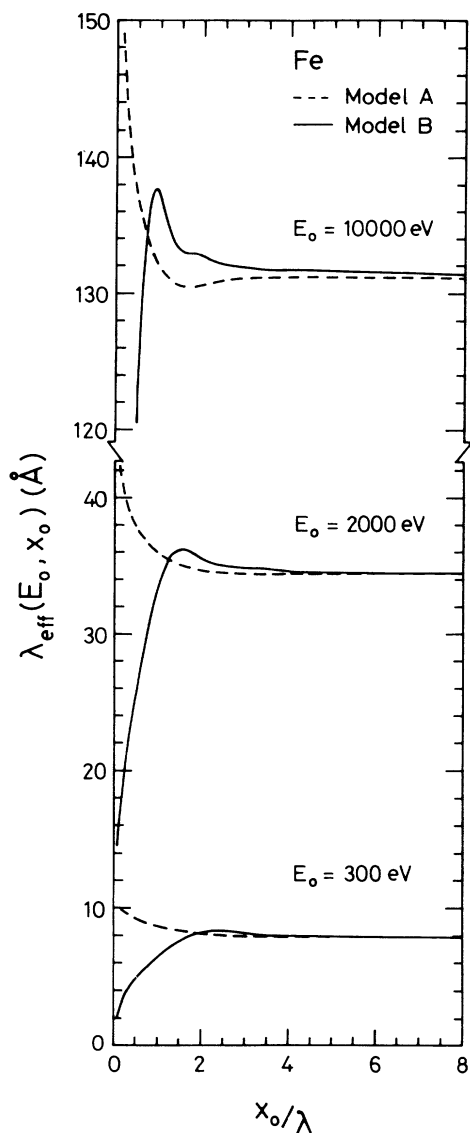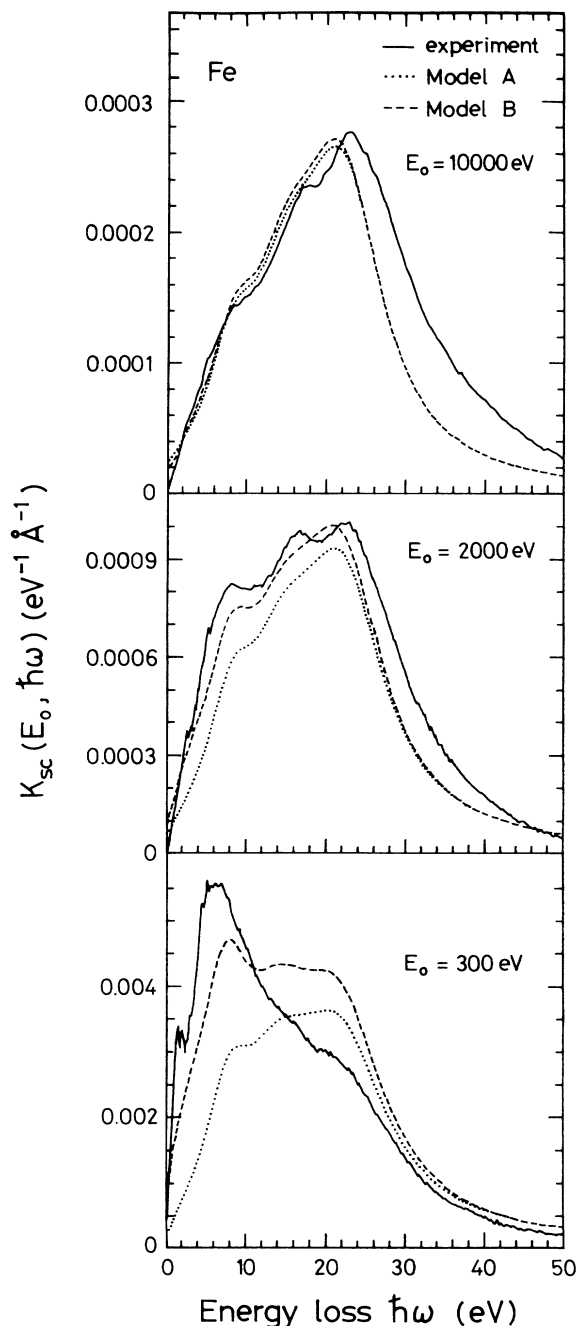

FIG. 7 Effective inelastic mean free paths [Eq. (22)] for electrons backscattered at different depths $a = x_0/2$ in Fe. Several primary electron energies E_0 are considered within the two models A and B.

FIG. 8. Theoretical cross sections from Eq. (20) for models A and B, with ϵ from Eq. (19) compared to experimental cross sections at several energies in Fe.

$K_{\text{eff}}(E_0,\hbar\omega,x_0)$ from Eq. (13) (model A) and Eq. (15) (model B), respectively. Model B reproduces the experimental cross sections better than model A, especially for low primary electron energies. For $E_0 = 10\,000$ eV, the two models give almost identical $K_{\text{sc}}(E_0,\hbar\omega)$. This is because for large E_0, the contribution from electrons that have traveled deep into the solid is relatively stronger, and in the limit $x_0 \to \infty$, $K_{\text{eff}}(E_0,\hbar\omega,x_0)$ is the same for both models (see Sec. II).

The only inputs in these calculations are the dielectric function (taken from optical data[20]) and the inelastic

mean free path (taken from Ref. 19). Thus no adjustable parameters have been applied. In spite of this, the *quantitative* agreement between model B and experiment is reasonable.

The dielectric function for Fe was taken as a fit to optical data[20] that unfortunately are only available in the energy range 0–30 eV. Improved agreement between theory for model B and experiment in Fig. 8 might be expected with a more complete dielectric function for Fe.

Similar calculations of $K_{\text{sc}}(E_0,\hbar\omega)$ were made for Ti, Cu, Pd, Ag, and Au as shown in Figs. 9–13. The experimental cross sections are also shown for comparison. Note that, for the theoretical calculations, no adjustable parameters have been applied, and that theory and experiment can be compared on an absolute scale.

In the experimental cross sections, the relative intensity of structure below ~ 15 eV increases with decreasing primary energy. The same trend is observed for both models A and B. However, this effect is stronger for model B and much closer to the behavior in the experimental cross sections than for model A. Furthermore,
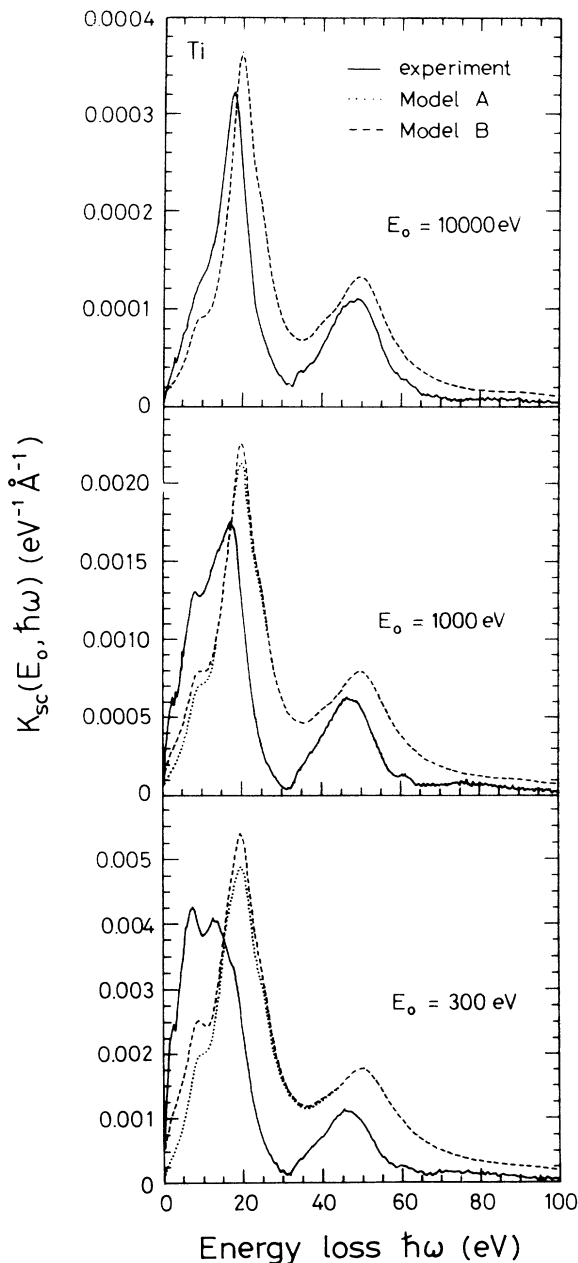
FIG. 9. Theoretical cross sections from Eq. (20) for models A and B with ϵ from Eq. (19) compared to experimental cross sections at several energies in Ti.
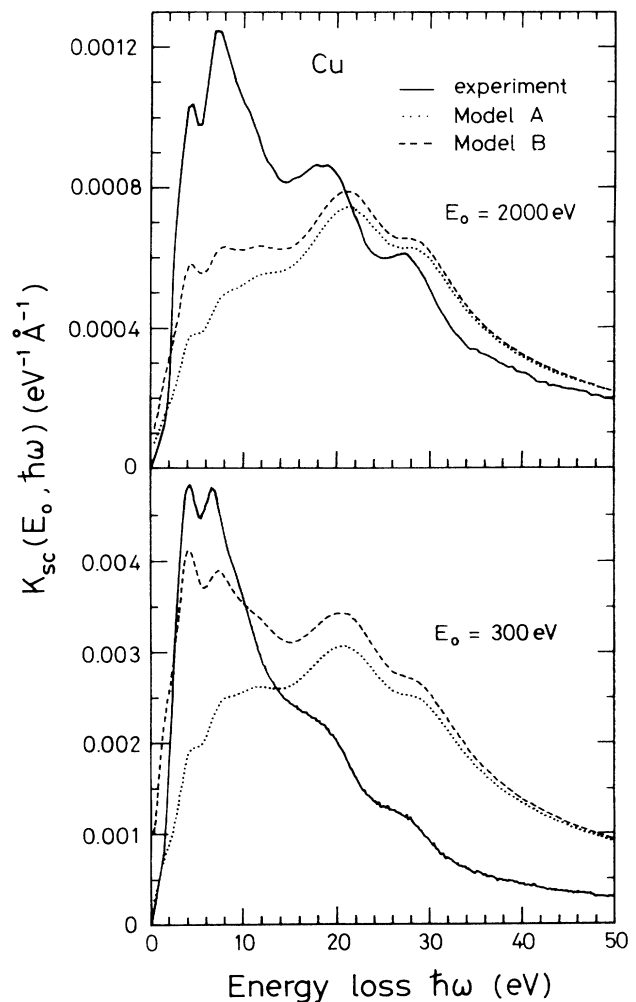
FIG. 10. Theoretical cross sections from Eq. (20) for models A and B with ϵ from Eq. (19) compared to experimental cross sections at several energies in Cu.

the overall quantitative agreement with experiment is for all metals and for all primary energies better for model B than for model A.

Although model B on an absolute scale gives a reasonable description of the experimental cross sections, the shape and the relative intensity of the various features are not reproduced. There are several possible reasons for this. For example, at $E_0 = 10\,000$ eV, one would expect a good agreement, because then the effect of the surface is small and we are close to the optical limit. The observed deviations at high primary energies therefore indicate that the applied dielectric functions are not perfect. Be-

sides, the k dependence of ϵ is not known and may be different from that assumed in Eq. (19).

Furthermore, the theoretical λ values may be in error by more than 10%.[19] This will affect the absolute scale of the experimental cross sections, and to a small extent the relative intensity of features at low- and high-energy loss in the theoretical calculations [see Eq. (20)].

Finally, in the experimental geometry, the angle of incidence was 20° and the exit angle was 15° (see Fig. 1 in Ref. 2), which therefore differs from the normal incidence and exit angles considered in the present calculations. This as well as surface roughness could be other sources of deviations.

Considering the combined influence of these effects, the agreement between cross sections from model B and experiment is reasonable.

It is suggested to apply the present model to determine the dielectric function $\epsilon(k=0)$ and thus to determine the optical properties of solids from REELS spectra. Thus, an iterative adjustment of ϵ in Eq. (8), until Eq. (20) gives a good match with an experimental REELS spectrum,
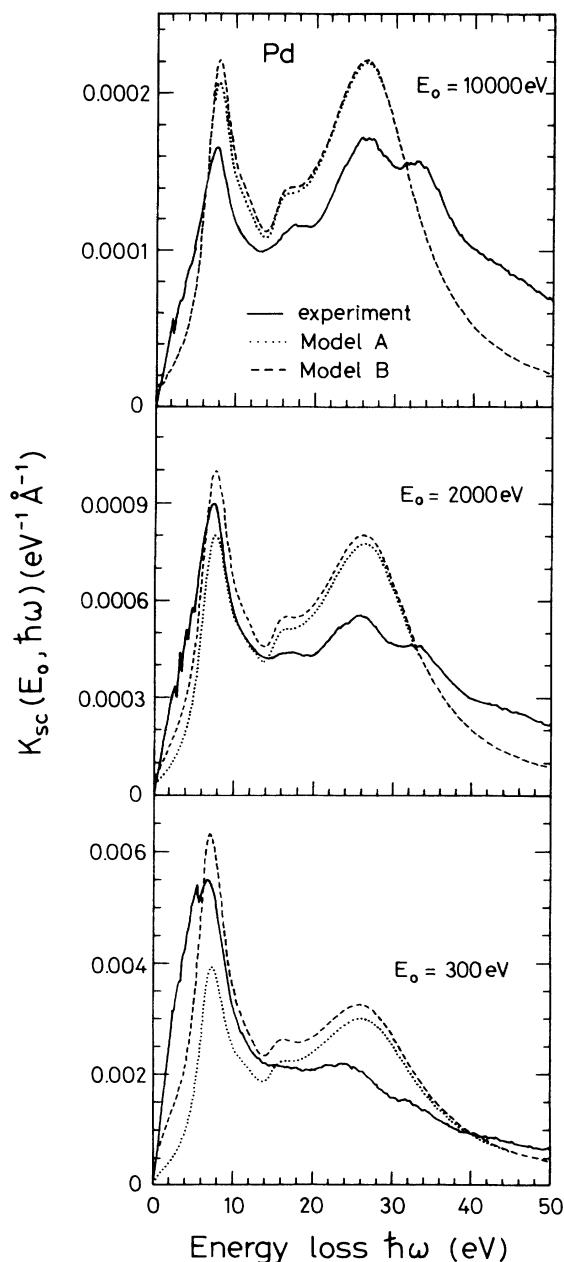

FIG. 11. Theoretical cross sections from Eq. (20) for models A and B with ϵ from Eq. (19) compared to experimental cross sections at several energies in Pd.
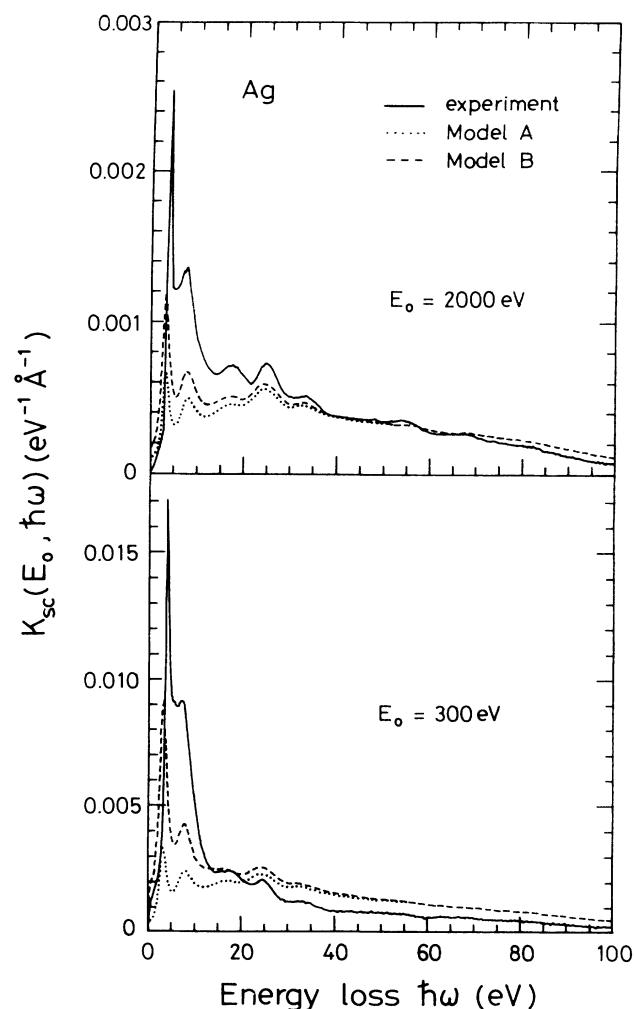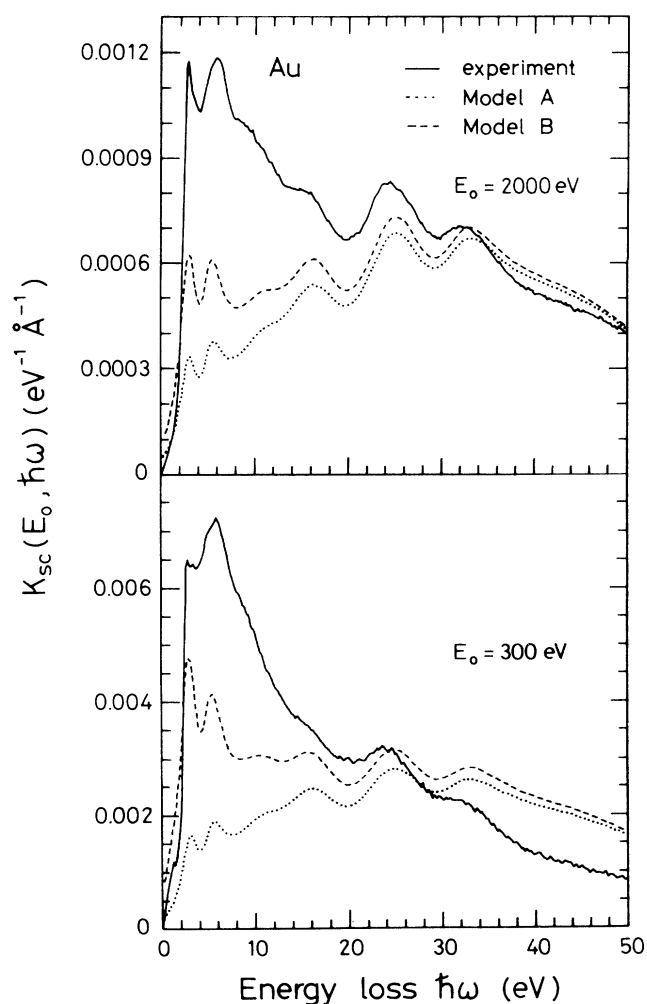
FIG. 12. Theoretical cross sections from Eq. (20) for models A and B with ϵ from Eq. (19) compared to experimental cross sections at several energies in Ag.

TABLE II. Parameters used to expand ϵ from Refs. 20–22 according to Eq. (19) with $k = 0$.

i	ħω_i	Cu 10²f_i	ħγ_i	ħω_i	Ag 10²f_i	ħγ_i	ħω_i	Au 10²f_i	ħγ_i
1	1.2	1.4	1.5	0.4	1.2	0.63	1.8	5	1.8
2	2.5	4.9	3.0	1.2	4.6	1.5	4.5	3	2.0
3	6.0	3.5	4.0	6.3	6.6	3.5	9.0	18	7.6
4	10.0	6.3	8.0	14.5	25.3	12.0	14.0	11	7.0
5	16.8	13.3	12.0	22.0	8.6	6.8	21.5	16	7.0
6	27.5	2.2	7.0	31.5	3.2	5.8	30.5	7	6.3
7	36.0	14	45.0	49.0	100	52.0	42.0	50	32.0
8	60.0	24.4	60.0	54.0	0.61	4.5			
9				67.0	1.5	5.0			
10				79.0	30.4	32.0			

i	ħω_i	Fe 10²f_i	ħγ_i	ħω_i	Ti 10²f_i	ħγ_i	ħω_i	Pd 10²f_i	ħγ_i
1	4.2	18.7	6.5	5.1	76.5	5.5	4.3	10.5	3.0
2	12.0	6.7	8.0	12.0	53.8	7.0	11.0	1.9	5.0
3	19.0	10.7	14.0	24.0	4.1	5.0	14.8	2.1	3.0
4				39.0	8.3	6.0	21.0	29.3	15.0
5				46.0	111	16.0			
6				90.0	15.5	20.0			

FIG. 13. Theoretical cross sections from Eq. (20) for models A and B with ϵ from Eq. (19) compared to experimental cross sections at several energies in Au.

determines the $\epsilon(k = 0)$ function, which, within the limitations of the formalism, is the dielectric function of the solid.

It is thus hoped that the present formalism will, in the future, increase the quantitative information that can be extracted from REELS experiments.

V. CONCLUSIONS

We have developed two models within the dielectric-response formalism to reproduce experimental inelastic-scattering cross sections determined from REELS spectra. It is found that a model which includes the k dependence of ϵ and the effect of the field set up by the incoming electron on the outgoing electron gives the best description of experimental cross sections of Al, Ti, Fe, Cu, Pd, Ag, and Au. Primary electron energies in the 175–10 000-eV energy range were investigated.

Inputs to the calculations for all metals except Al are the dielectric function and the inelastic electron mean free path, which were both taken from previous works. Even without any adjustable parameters, the quantitative

TABLE III. Inelastic mean free paths λ for the elements at different energies [taken from Tanuma, Powell, and Penn (Ref. 19)]. Besides $\lambda = 23.2$ Å for Ti at 1000 eV (Ref. 19) was used. For $E_0 = 10\,000$ eV, the TPP2 formula (Ref. 19) was applied. The plasmon energies (Ref. 19) are also shown.

	E_0 (eV)	Fe	Pd	Ti	Cu	Ag	Au
λ (Å)	300	7.2	7.8	9.5	7.7	6.4	6.0
	2 000	27.7	30.9		27.7	24.0	21.6
	10 000	104	116	154			
$\hbar\omega_p$ (eV)		30.6	30.6	17.7	35.9	29.9	29.8

agreement between theory and experiment is reasonable. The effective inelastic mean free path for a backscattered electron was found to depend strongly on the path length. Possible sources of error were discussed. A method to determine the dielectric function from REELS spectra was suggested.

ACKNOWLEDGMENTS

*Permanent address: Departamento de Física Aplicada C-XII, Universidad Autónoma de Madrid, E-28049 Madrid, Spain.

[1]S. Tougaard and I. Chorkendorff, Phys. Rev. B **35**, 6570 (1987).

[2]S. Tougaard and J. Kraaer, Phys. Rev. B **43**, 1651 (1990).

[3]J. Lindhard, K. Dan. Vidensk. Selsk. Mat. Fys. Medd. **28**, 8 (1954).

[4]R. H. Ritchie, Phys. Rev. **106**, 874 (1957).

[5]J. Daniels, C. V. Festenberg, H. Raether, and K. Zeppenfeld, in *Springer Tracts in Modern Physics,* edited by G. Holer (Springer-Verlag, Berlin, 1970), Vol. 54.

[6]G. Chiarello, E. Colavita, M. De Crescenzi, and S. Nannarone, Phys. Rev. B **29**, 4878 (1984).

[7]Y. Ohno, Phys. Rev. B **39**, 8209 (1989).

[8]J. C. Ingram, K. W. Nebesny, and J. E. Pemberton, Appl. Surf. Sci. **44**, 279 (1990).

[9]F. Yubero, J. M. Sanz, E. Elizalde, and L. Galán, Surf. Sci. **237**, 173 (1990).

[10]C. J. Powell, Phys. Rev. **175**, 972 (1968).

[11]F. Yubero and S. Tougaard, Surf. Interf. Anal. (to be published).

[12]R. H. Ritchie and A. Howie, Philos. Mag. **36**, 463 (1977).

[13]S. Tougaard and B. Jørgensen, Surf. Sci. **143**, 482 (1984).

[14]H. Raether, *Excitation of Plasmons and Interband Transitions by Electrons,* Springer Tracts in Modern Physics (Springer-Verlag, Berlin, 1982), p. 42.

[15]S. Tougaard, Surf. Interf. Anal. **11**, 453 (1988).

[16]D. R. Penn, Phys. Rev. B **13**, 5248 (1976).

[17]D. R. Penn, J. Electron. Spectrosc. Relat. Phenom. **9**, 29 (1976).

[18]C. J. Tung and R. H. Ritchie, Phys. Rev. B **16**, 4302 (1977).

[19]S. Tanuma, C. J. Powell, and D. R. Penn, Surf. Interf. Anal. **17**, 911 (1991).

[20]J. H. Weaver, C. Krafka, D. W. Lynch, and E. E. Koch, Physics Data, Optical properties of metals (Fachinformationszentrum Energie, Physik, Matematik G.m.b.H., Karlsuhe, 1981) No. 18 (ISSN 0344-8401).

[21]C. Wehenkel and B. Gauthé, Phys. Status Solidi B **64**, 515 (1974).

[22]C. Wehenkel, J. Phys. (Paris) **36**, 199 (1975).